Far-Infrared Spectra of Yttrium-Doped Gold Clusters Au_nY ($n = 1$–9)

Ling Lin,[b] Pieterjan Claes,[c] Philipp Gruene,[a] Gerard Meijer,[a] André Fielicke,*[a] Minh Tho Nguyen,*[b] and Peter Lievens*[c]

The geometric, spectroscopic, and electronic properties of neutral yttrium-doped gold clusters Au_nY ($n = 1$–9) are studied by far-infrared multiple photon dissociation (FIR-MPD) spectroscopy and quantum chemical calculations. Comparison of the observed and calculated vibrational spectra allows the structures of the isomers present in the molecular beam to be determined. Most of the isomers for which the IR spectra agree best with experiment are calculated to be the energetically most stable ones. Attachment of xenon to the Au_nY cluster can cause changes in the IR spectra, which involve band shifts and band splittings. In some cases symmetry changes, as a result of the attachment of xenon atoms, were also observed. All the Au_nY clusters considered prefer a low spin state. In contrast to pure gold clusters, which exhibit exclusively planar lowest-energy structures for small sizes, several of the studied species are three-dimensional. This is particularly the case for Au_4Y and Au_9Y, while for some other sizes ($n = 5$, 8) the 3D structures have an energy similar to that of their 2D counterparts. Several of the lowest-energy structures are quasi-2D, that is, slightly distorted from planar shapes. For all the studied species the Y atom prefers high coordination, which is different from other metal dopants in gold clusters.

Introduction

There has been considerable interest in gold clusters, in part due to their potential applications in a wide variety of areas, for example as catalysts for CO oxidation reactions,[1,2] or as material for tips and contacts in molecular electronic devices.[3] Most of the recent theoretical studies focused on their geometrical and electronic structure, as there is evidence that details of the geometry and the dimensionality (planar or three dimensional) of small Au_n clusters are closely linked to their catalytic activities.[4–6] Earlier quantum chemical studies showed that small neutral Au_n clusters prefer planar geometries and a 2D–3D transition occurs at a size of $n = 12$.[7,8] For the corresponding cations Au_n^+ and anions Au_n^-, the structures have been found experimentally and theoretically to be planar up to $n = 7$ and $n = 11$, respectively.[9–12] The preference for the 2D form has been interpreted as a consequence of relativistic effects,[13,14] which causes shrinking of the size of s atomic orbitals, and subsequently enhances the s–d hybridization and d–d interaction in gold atoms, thus resulting in a consistent preference for more directional Au–Au bonds.[15]

It is known that the doping of a metal cluster by another atom can fundamentally modify the cluster properties, either its shape or its electronic and magnetic properties. Up to now, numerous studies on doped gold clusters have been carried out, with dopant atoms ranging from nonmetallic elements (S, P, Si, Se…)[10,16–23] to alkali metals (Li, Na…)[21,24,25] and transition metals (Sc, Ti, V…).[26–43] Small Au_nS clusters[16] were calculated to exhibit planar structures and their geometry can be constructed by replacing one Au atom of the Au_{n+1} cluster by a S atom, while from $n = 6$ on, the doped cluster adopts a 3D structure. Au_5S was predicted to have higher stability than its neighbors. For Au_nSi ($n = 1$–8),[17] the 3D structures start earlier

from $n = 3$, which is accounted for by the strong directional covalent bonding resulting from a significant contribution of the p electrons of Si. Within this series, Au_4Si was found to adopt a T_d structure and to show extraordinary stability.[17,18] In an earlier study on Au_5M, with M = Na, Mg, Al, Si, P, and S, it was predicted that dopant atoms with s electrons (Na, Mg) yield planar structures similar to that of Au_6, whereas those with p electrons (Al, Si, P) result in nonplanar structures with an exception for S.[21]

Transition-metal-doped gold clusters have received much more attention. A systematic theoretical study on Au_nZn ($n \leq 6$)[26] showed that all the lowest-energy isomers are planar, and structurally resemble the pure gold clusters Au_{n+1}. Moreover,

[a] Dr. P. Gruene, Prof. Dr. G. Meijer, Dr. A. Fielicke
Fritz-Haber-Institut der Max-Planck-Gesellschaft
Faradayweg 4–6, 14195 Berlin (Germany)
Fax: (+ 49) 30-8413-5603
E-mail: fielicke@fhi-berlin.mpg.de

[b] Dr. L. Lin, Prof. Dr. M. T. Nguyen
Department of Chemistry and
Institute for Nanoscale Physics and Chemistry (INPAC)
Katholieke Universiteit Leuven
3001 Leuven (Belgium)
Fax: (+ 32) 16-327992
E-mail: minh.nguyen@chem.kuleuven.be

[c] P. Claes, Prof. Dr. P. Lievens
Laboratory of Solid State Physics and Magnetism, and INPAC
Katholieke Universiteit Leuven
3001 Leuven (Belgium)
Fax: (+ 32) 16-327983
E-mail: peter.lievens@fys.kuleuven.be

stable isomers tend to equally delocalize their valence s electrons over the entire skeleton and thereby maximize the number of Au—Zn bonds within the structure. Subsequently, the Au_5Zn^+ cation was reported to be the first example of a σ-aromatic bimetallic cluster, which was proposed to cause its enhanced stability.[27] The properties of Au_nM with $n = 2$–7 and M = Ni, Pd, and Pt have been studied theoretically.[28] The planar structures are again favorable for all the clusters studied, except for Au_7Ni, for which the most stable 3D structure turns out to be almost degenerate with its corresponding 2D form. The stability and electronic properties of Ni-doped gold clusters were found to be similar to those of pure gold clusters, but with increased bond lengths. In contrast, the addition of Pd and Pt changes the electronic properties, due to strong d–d or s–d interactions between the impurity and host atoms.[28] Another theoretical study on AuPt and Au_6Pt[29] suggested that doping of Pt in Au clusters would change the chemical reactivity, due to the significant contribution of Pt 5d orbitals to the frontier molecular orbitals of the binary species. Studies on neutral and anionic $M@Au_6$ (M = Ti, V, Cr) showed that all the clusters prefer to be planar with the transition metal located at the center of a Au_6 ring, and the magnetic moments of the impurity atoms not being quenched by the nonmagnetic gold host.[30] A more recent quantum chemical study on Au_nTi ($n = 2$–16)[31] also found the most stable structures in the size range $n = 2$–7 to be planar, which is different from previous studies showing that Au_4Ti has a T_d structure.[32,33] The geometrical transition from 2D to 3D was predicted to occur at $n = 8$, whereas the larger clusters with $n = 12$–16 prefer cages, with the Ti atom located in the middle of the Au cage.[31] There have been several other studies on larger Au_nM clusters with $n \geq 12$,[34–43] which consistently showed that doping of gold clusters is indeed a powerful way of tuning their chemical and physical properties.

The theoretical identification of the global minimum structure of clusters becomes increasingly complicated for larger cluster sizes. This holds especially true for doped species, for which the number of possible isomers becomes substantially larger. Nonetheless, most of the above-cited studies refrained from using global optimization schemes,[44] in part due to the high computing demands. In this situation, experimental results that can verify theoretical predictions are highly desirable. In earlier mass spectrometric studies of the properties of Au_nM^+ (M = Sc, Ti, V, Cr…, $n = 1$–40), the observed stability patterns were discussed on the basis of a phenomenological shell model[45–47] that takes into account the electronic structure of the dopant atom.[27,48] The enhanced abundance for Au_5X^+, where X = V, Cr, Mn, Fe, Co, and Zn, was rationalized in terms of their planarity in combination with the six delocalized electrons being a magic number for 2D systems.[49,50]

In this series of photofragmentation mass spectrometry experiments strong abundance enhancements also were observed for 16-atom gold-cluster cations doped with a trivalent metal (Sc, Y, Nb).[48,51,52] The enhanced stability corresponds to an 18-electron shell closure which is strengthened by a wine-bottle-type mean-field potential resulting from the endohedral position of the dopant atom in the gold.

Photoelectron spectroscopic studies have focused on the structures of anionic gold cages of 12 atoms doped with W and Mo,[39] V, Nb, and Ta,[40] anionic gold cages of 16 and 17 atoms doped with Cu,[41] and anionic cages of 16 gold atoms doped with Fe, Co, Ni, Ag, Zn, In,[42,43] and the main-group elements Si, Ge, and Sn.[22] For Au_{16} species doped with Fe, Co, and Ni, detailed structural information was obtained with trapped-ion electron diffraction.[42] While all transition-metal atoms are located inside the gold cage,[39–43] Si becomes part of it, but Ge and Sn are found on the surface of the cages.[22] Recently, this study has been extended to smaller anionic gold clusters containing 5–8 atoms and a Si, Ge, or Sn dopant atom.[23]

In this work we set out for a combined experimental and theoretical investigation to explore the structural properties of small yttrium-doped gold Au_nY clusters, with n ranging from 1 to 9. The primary objective is twofold. The first is to record their experimental vibrational spectra using far-infrared multiple photon dissociation (FIR-MPD) spectroscopy. These spectra are inherently sensitive to the structure of their complexes with the messenger xenon atom. The second is to interpret the recorded spectra with the aid of quantum chemical calculations. This combined approach has been shown to be successful for identifying the structure of cationic silicon clusters and for explaining the influence of copper and vanadium doping on their structures.[53,54] Furthermore, FIR-MPD has recently been used to determine the geometry of pure neutral gold clusters (Au_n with $n = 7$, 19, and 20) for the first time.[55] A few studies also exist on Au_nY, including experimental studies on the stability of their cations Au_nY^+,[51,52] and a theoretical study devoted to the structure of neutral Au_nY using density functional theory (DFT) with the B3LYP functional and the LANL2DZ basis set.[56] Also, a quantum chemical study on gold clusters doped with two yttrium atoms was reported.[57] We have recently reported on the properties of small $Au_{4-6}Y$ clusters and predicted that the Au_6Y^- anion is a σ-aromatic six-membered ring.[58] In the present work, we use far-IR spectroscopy and quantum chemical calculations to investigate systematically the geometric, electronic, and bonding properties of neutral Au_nY ($n = 1$–9) clusters.

Experimental and Computational Methods

The FIR-MPD experiments were performed in a cluster beam setup that was coupled to a beamline of the Free Electron Laser for Infrared eXperiments (FELIX) at the FOM Institute for Plasma Physics Rijnhuizen, in Nieuwegein, The Netherlands.[53,59–62] For the production of binary Au_nY clusters, a pulsed (10 Hz) dual-target dual-laser vaporization source was implemented in the setup.[63] Following vaporization of the two target materials, condensation took place in a mixture of helium and isotopically enriched xenon (0.8 % ^{129}Xe in He), and yttrium-doped gold clusters were formed and passed through a copper channel. Cluster–xenon complexes were observed when this channel was cooled to 130 K. The molecular beam containing these complexes passed through a skimmer and an aperture of diameter 1 mm, which was located in front of the acceleration electrodes of a reflectron time-of-flight mass spectrometer. Vibrational spectroscopy was performed using action

spectroscopy with the messenger atom technique.[64,65] The molecular beam was overlapped with the counter-propagating pulsed (5 Hz) far-IR beam provided by FELIX, which was loosely focused behind the aperture. At a vibrational resonance of a given complex, the xenon ligand could be evaporated resulting in a depletion of the complex intensity in the molecular beam. While all charged species were blocked from entering the mass spectrometer due to a constant voltage applied to the aperture, neutral clusters were ionized by means of an F_2-excimer laser (7.9 eV photon^{-1}) between the acceleration plates. The depletion spectra were obtained by comparing the ion intensities of the doped gold–xenon complexes with and without FELIX as a function of the FELIX frequency.[66] In the figures showing FIR-MPD spectra, the raw data points are plotted as dots while a gray line connects their three point moving average.

For quantum chemical calculations, initial geometry optimizations and subsequent determination of the harmonic vibrational frequencies were carried out using DFT with the pure BP86 functional[67–69] and the correlation-consistent cc-pVDZ-PP basis set,[70–72] where PP stands for an effective core potential replacing the cores. To improve the calculated relative energies, single-point electronic energy calculations were carried out for some low-lying isomers of Au_nY with the coupled-cluster theory CCSD(T)[73] in conjunction with the larger cc-pVTZ-PP basis set,[70–72] on the basis of BP86/cc-pVDZ-PP optimized structures. The PP basis sets cc-pVnZ-PP ($n = D$ and T) employed here already include the relativistic effects that are crucial in the treatment of heavy elements such as gold. For each isomeric system, a large number of geometries with different spin states were considered. When treating open-shell systems, the spin–orbit coupling also needs to be considered. However, the contributions of the spin–orbit effects to the relative energies are much smaller than the inherent errors of the DFT method. To calibrate the calculated DFT results for some small systems, coupled-cluster theory CCSD(T) calculations were also performed. The comparison will be given in the following discussion. All calculations were performed with the Gaussian 03[74] and MOLPRO 2006.1[75] program packages. The natural bond orbital (NBO) charges will be used for the discussion of the charge distribution in Au_nY, and they were computed by using the NBO 5.G code[76] integrated into the Gaussian program suite.[74]

The calculated stick spectra are folded with a Gaussian line width function of 4 cm^{-1} full width at half maximum for ease of comparison with the experimental spectra. Under current practice, harmonic vibrational frequencies ($\tilde{\nu}$) obtained by DFT calculations are often scaled to improve the agreement with experimental IR results. For the smaller cluster Au_4YXe, its unscaled calculated vibrational spectrum only marginally deviated from experiment.[58] However, as the cluster size increased, larger deviations appeared, thus showing that the DFT method employed systematically underestimates the frequencies with growing cluster size.[54] This implies that the often-used procedure of including a constant scaling factor will not result in optimal agreement between theory and experiment for both high- and low-frequency modes. Therefore, we employed the following—albeit somewhat arbitrary—linear scaling relation [Eq. (1)]:

$$\tilde{\nu} = 22\,\text{cm}^{-1} + \tilde{\nu}_{calc} \times 0.94 \qquad (1)$$

which was obtained by fitting the largest frequencies of the vibrational spectrum for Au_nY–Xe complexes with the experimental values (Table S1 in the Supporting Information).

A similar scaling formula has been used to scale frequencies of cationic niobium oxide clusters, although in that case the fitting could be performed on well-characterized reference systems.[60] In Table S2 in the Supporting Information a comparison is made between the theoretical frequencies scaled this way, with the optimal scaling factors for each mode as obtained from the experimental line positions, and computed values corresponding to the assigned ground-state structures. Use of a single scaling factor of 1.06, obtained by averaging the optimal ratios for the largest frequencies (Table S2 in the Supporting Information), would not alter the interpretations and structural assignments, but results in somewhat poorer agreement. Although the scaling using Equation (1) leads to reasonable agreement with experiment, it should be stressed that there is no obvious physical explanation for the fairly large scaling needed to obtain agreement for the low-energy vibrational frequencies. This is a well-known problem that is often encountered for harmonic vibrational frequency computations with (DFT-based) quantum chemical approaches.[77]

Results and Discussion

In the following we will discuss the geometric and spectroscopic properties of yttrium-doped gold clusters, by using the combined strength of FIR-MPD experiments and quantum chemical calculations. In the experiment the source conditions were optimized to form mainly cluster complexes with a single Xe atom as a messenger atom; however, for some sizes (Au_nY, $n = 4$, 5, 7, 8), attachment of a second Xe atom is also observed. It appears that this second Xe atom can influence the geometry of the cluster and this will be analyzed in detail. Such effects of rare-gas attachment on the structures of clusters have been reported before.[65,78]
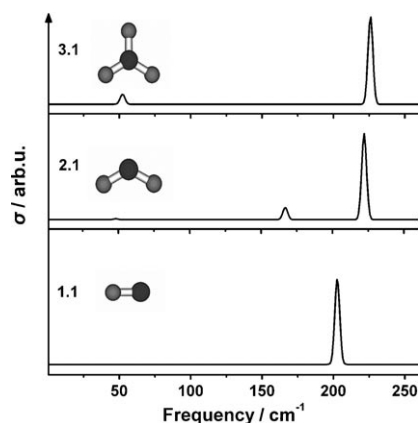
AuY, Au₂Y, and Au₃Y

Experimental spectra of the three smallest clusters were not recorded as their Xe complexes are not observed, probably because of their high ionization energy, and therefore only calculated results are presented in this section. The average Au—Y bond lengths are listed in Table S1 in the Supporting Information. Figure 1 displays the optimized geometries whereas Figure 2 shows calculated vibrational spectra. A number of interesting properties can be noted as follows:

i) The diatomic AuY prefers a low-spin singlet $^1\Sigma^+$ ground state, and the lowest-lying triplet $^3\Sigma^-$ state is 0.33 eV higher in energy (Figure 1). In both the HOMO and LUMO, the largest lobe is centered at the Y atom (see Figure S1 in the Supporting Information).

ii) The triatomic Au₂Y exhibits a C_{2v} form in which the Y atom occupies the central position (AuYAu). Again the largest components of both frontier orbitals are centered at the Y atom resulting in a doublet ground state $^2A_1$. The alternative isomer AuAuY is found to be 1.73 eV higher in energy. The Au—Y bond length of 2.653 Å in AuYAu is slightly larger than that in AuY, in which the length is 2.627 Å (Table S1 in the Supporting Information). In the quartet
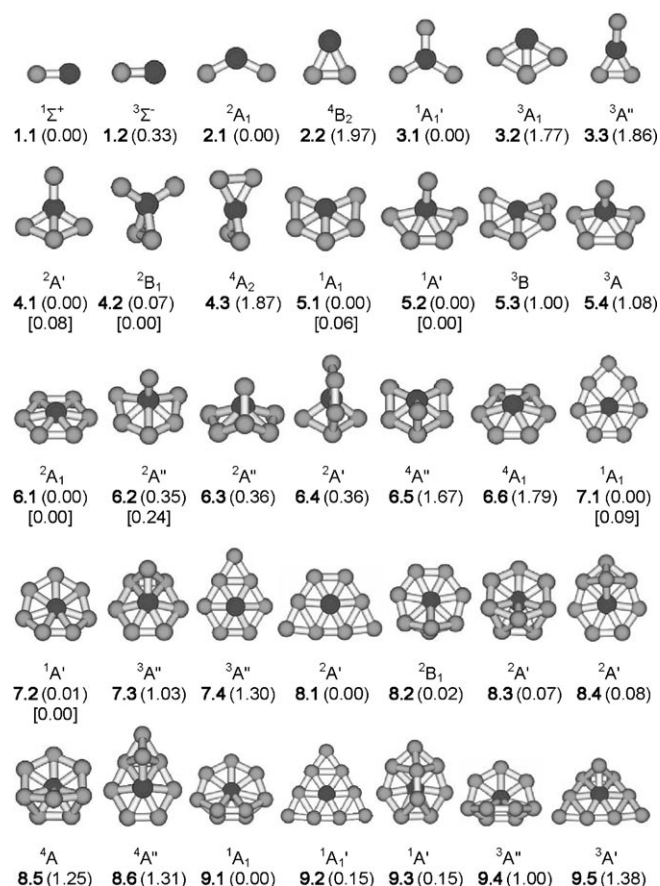
Figure 1. Structures of the low-lying isomers of Au$_n$Y ($n = 1$–9) in their respective electronic ground state, selected triplet or quartet states (grey spheres: gold; dark spheres: yttrium), and their relative energies (in eV, at the BP86/cc-pVDZ-PP level of theory; CCSD(T)/cc-pVTZ-PP values are given in square brackets, including zero-point energy corrections).

Figure 2. Vibrational spectra of AuY, Au$_2$Y, and Au$_3$Y calculated at the BP86/cc-pVDZ-PP level. σ = intensity.

manifold, Au$_2$Y is a triangle ($^4B_2$), similar to the pure Au$_3$ cluster, but ~1.97 eV above the ground state $^2A_1$.

iii) The tetraatomic Au$_3$Y cluster is characterized by a highly symmetric structure (D_{3h}) with, once more, Y in the central position. The $^1A_1'$ state is favored over the triplet counterpart. In the singlet state, the largest components of the

HOMO are located on Au whereas in the LUMO they are on Y. In this case, the Au–Y bond length (2.656 Å) is similar to that of Au$_2$Y (2.653 Å). In the triplet state, the D_{3h} form is distorted towards a C_s structure ($^3A''$) which is 1.86 eV above the singlet state. Nevertheless, a C_{2v} rhombic form ($^3A_1$), with a similar shape to the pure Au$_4$ cluster, becomes slightly lower in energy being ~1.77 eV above the singlet (Figure 1).

Regarding the vibrational spectra displayed in Figure 2, the most intense bands corresponding to the Au–Y stretching vibrations are centered at 202 (AuY), 222 (Au$_2$Y), and 226 cm^{-1} (Au$_3$Y), and a frequency shift towards the blue takes place as the size of the cluster increases.

Au$_4$Y

The IR spectra of these cluster–rare-gas complexes are recorded upon photodissociation of a cluster complex with xenon as the messenger atom. As mentioned above, both complexes with one and two Xe atom(s) are observed in the experimental mass spectra. To evaluate the effect of xenon, vibrational spectra of both the bare Au$_n$Y clusters and their Xe complexes were calculated. We can now examine the influence of Xe. Figure 3 shows a comparison of the far-IR spectrum of Au$_4$YXe
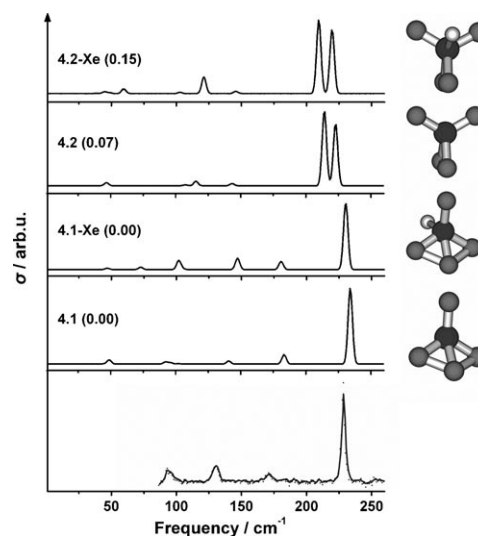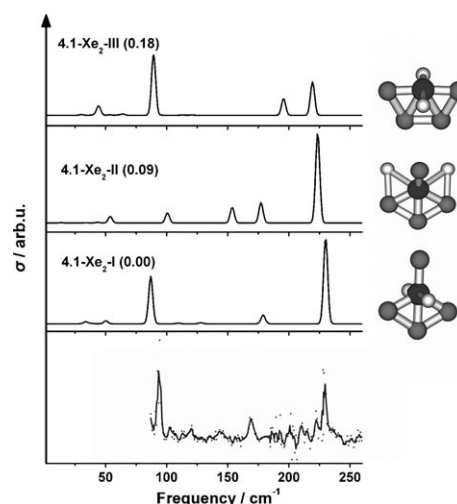

Figure 3. Comparison of the calculated (BP86/cc-pVDZ-PP) vibrational spectra of the two lowest-lying Au$_4$Y isomers (light spheres with asterisk: xenon; grey spheres: gold; dark spheres: yttrium) and the corresponding Xe complexes with the experimental FIR-MPD spectrum of Au$_4$YXe (bottom). The relative energies are given in eV.

and the calculated spectra of the two lowest-lying isomers of Au$_4$Y, denoted as **4.1** and **4.2**, as well as their corresponding Xe complexes. Again, the Y atom is situated at the center of the Au$_4$Y cluster, bound to all four Au atoms. However, because of a strong Jahn–Teller effect arising from the degenerate orbital occupancy due to the unpaired electron, the geometry of Au$_4$Y is distorted from an ideal T_d point group symmetry, which leads to less symmetric C_s (**4.1**) and C_{2v} (**4.2**) struc-

tures. The shapes of their frontier orbitals are shown in the Supporting Information (Figure S1). Both equilibrium structures **4.1** (^{2}A′) and **4.2** (^{2}B$_1$) are calculated to be nearly degenerate (Figure 1). Xenon can be attached either to the Y of **4.1** with a binding energy of 0.14 eV, or to one of the Au atoms with a much smaller binding energy of ~0.02 eV. The binding energies of Xe to Y and the Au of **4.2** are 0.06 and 0.04 eV, respectively. Therefore, the Y-attached **4.1-Xe** complex is energetically preferred, and we will take it as an example to understand the influence of Xe on the vibrational spectra. From Figure 3, one finds that upon Xe attachment, the most intense band of the **4.1** isomer at 234 cm^{-1} and the weak band at 183 cm^{-1} in the vicinity are slightly red-shifted to 230 and 180 cm^{-1}, respectively, whereas the weak bands at 49, 92, and 140 cm^{-1} are blue-shifted to 72, 102, and 147 cm^{-1}. At the same time we also observe small changes in band intensities. As can be expected from the weak interaction energy, attachment of Xe to Au atoms only has a limited influence on the vibrational spectrum (Figure S2 in the Supporting Information). Similar effects of Xe have also been found for **4.2** and most of the other low-lying isomers of Au$_n$Y (n = 5–9).

Comparison of the calculated spectra of both lowest-energy Au$_4$Y isomers **4.1** and **4.2** and their corresponding complexes with single Xe atoms with the experimental results points out that most of the IR spectral features are reproduced in the simulated spectrum of **4.1-Xe**. The predicted IR intensities are also qualitatively correct. This demonstrates that **4.1-Xe** is the dominant isomer present in the molecular beam, whereas **4.2-Xe**, which lies 0.15 eV higher in energy than **4.1-Xe** at the BP86/cc-pVDZ-PP level, does not apparently contribute to the spectrum.

As mentioned above, we were also able to form the complex with two Xe atoms. At first, from the experimental IR spectrum only, it appears to have similar features to those for the complex with only one Xe atom attached, but the band intensities change significantly. However, the calculations find that addition of the second Xe atom enhances the geometrical symmetry from C_s (for Au$_4$YXe) to C_{2v} (for Au$_4$YXe$_2$), and therefore the Xe plays an important role and may not be ignored. The comparison between experimental and calculated IR spectra (see Figure 4) illustrates this important role of the second Xe atom. Although, at a first glance, both Au$_4$YXe and Au$_4$YXe$_2$ have a band around 90 cm^{-1}, the origin of this vibrational mode is completely different. Due to the presence of the second Xe atom, a blue shift is induced causing a lower band to be shifted from 72 to 87 cm^{-1}. For **4.1-Xe** the experimental band at 90 cm^{-1} is assigned to in-plane bending of the Au$_3$Y subunit (Movie S1 in the Supporting Information) while, due to the blue shift for **4.1-Xe$_2$-I**, the vibration of yttrium out of the plane, on the axis of the two Xe atoms, is also located around 90 cm^{-1} (Movie S2 in the Supporting Information). Thus, the IR spectrum of Au$_4$YXe changes upon attachment of a second Xe atom. This change is due to the increase in the cluster symmetry. From the comparison of the calculated IR spectra of the Xe$_2$ complexes with the experimental results (see Figure 4) we assign **4.1-Xe$_2$-I** as the most contributing isomer to the IR spectrum.
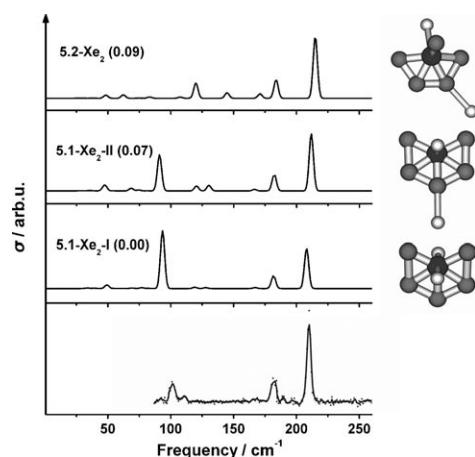

Figure 4. Comparison of the calculated (BP86/cc-pVDZ-PP) vibrational spectra of the three lowest-lying Au$_4$YXe$_2$ isomers (relative energies in eV are given in parentheses) with the experimental FIR-MPD spectrum.

Au$_5$Y

Figures 5 and 6 compare the experimental and predicted vibrational spectra of Au$_5$YXe and Au$_5$YXe$_2$, respectively. The two most stable isomers of Au$_5$Y, denoted as **5.1** and **5.2** (see Figure 1), are again almost degenerate in energy, with an energy difference of 0.00 and 0.06 eV by BP86 and CCSD(T) calculations, respectively. Both isomers have a central Y atom, but the shape of their frontier orbitals differs greatly from each other (Figure S1 in the Supporting Information). Compound **5.1** is in a ^{1}A$_1$ state with a planar shape (C_{2v}), and the corresponding triplet (**5.3**) is slightly distorted to a C_2 form (^{3}B) and markedly higher in energy by 1.00 eV above **5.1**. While **5.2** has a C_s ground state ^{1}A′, the triplet counterpart (**5.4**) loses symmetry (^{3}A) and lies 1.08 eV higher in energy than **5.1**, as indicated in Figure 1. While both **5.1** and **5.2** are basically degenerate in energy, the binding energies of Xe to Y in **5.1** and **5.2** are 0.14 and 0.10 eV, respectively. Therefore, **5.1-Xe** is slightly preferred
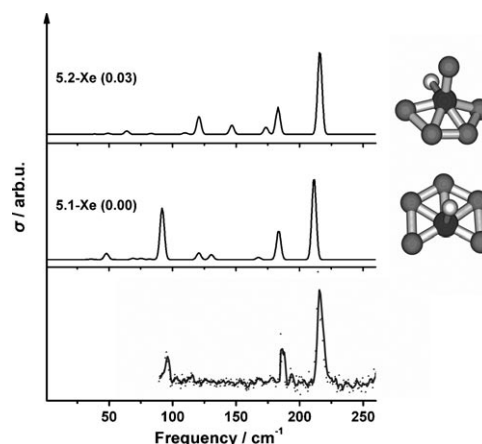
Figure 5. Comparison of the calculated (BP86/cc-pVDZ-PP) vibrational spectra of the two lowest-lying Au$_5$YXe isomers (relative energies in eV are given in parentheses) with the experimental FIR-MPD spectrum.

Figure 6. Comparison of the calculated (BP86/cc-pVDZ-PP) vibrational spectra of the three lowest-lying Au_5YXe_2 isomers (relative energies in eV are given in parentheses) with the experimental FIR-MPD spectrum.

energetically. As shown in Figure 5, the vibrational features of **5.1-Xe** and **5.2-Xe** are similar, especially for the two bands between 175 and 225 cm^{-1}. Accordingly, the experiment does not allow both isomers to be distinguished from each other easily, nor is it possible to exclude the fact that the measured spectrum actually consists of a superposition of both. However, a superposition of the **5.1-Xe** and **5.2-Xe** complexes should be visible as a double peak around 210 cm^{-1}. Only one peak is detected in the IR spectrum, which indicates that probably one of the isomers is the sole component in the molecular beam. The finding that **5.1-Xe** is slightly lower in energy than **5.2-Xe** favors the former structure. Furthermore, details of the vibrational spectrum corroborate this assignment. Following the scaling of the computed harmonic frequencies with the procedure including all investigated species as outlined above, the low-frequency component of **5.1** clearly fits better to the observed weak vibrational mode at 90 cm^{-1}. Therefore we conclude that **5.1-Xe** is the main carrier of the experimental spectrum, a claim that was not made in our earlier paper.[58]

Yet again, the complex with two Xe atoms was observed in the mass spectra and its IR photodissociation spectrum was recorded. Figure 6 shows a clear distinction between the calculated IR spectra of **5.1-Xe$_2$** and **5.2-Xe$_2$** complexes. Comparison of these calculated spectra with the experimentally obtained IR spectrum allows us to identify the cluster geometry as **5.1-Xe$_2$**, because the vibrational mode at 90 cm^{-1} is missing in **5.2-Xe$_2$**. We can also state that the second Xe atom is more likely to attach to the yttrium instead of the gold. It appears that only a single isomer of the Xe complex is present, otherwise a double peak should be visible around 210 cm^{-1}, which does not appear in the MPD experiment.

The behavior upon adding one or two Xe atoms to the cluster is different for Au_5Y compared with Au_4Y. In the case of Au_5Y, the cluster geometry is already more symmetric with respect to Au_4Y, namely C_{2v} and C_s, respectively. The addition of one or two Xe atoms does not have a large influence on the geometrical properties of the Au_5Y cluster, as it is already sym-

metric. This is also visible in the experimental IR spectra. We do not see a completely different IR spectrum. The general appearance of the vibrational spectrum remains the same, only a small blue shift is observed around 90 to 100 cm^{-1}. In the case of Au_4Y, more obvious changes in the spectra occur upon addition of a second Xe atom.
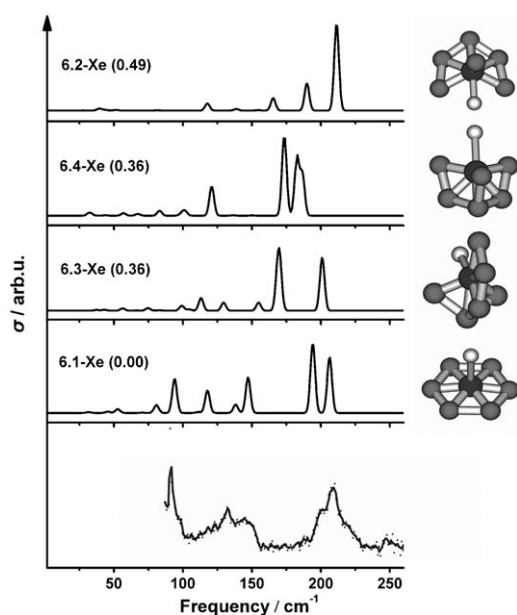
Au_6Y

The four structures **6.1**–**6.4** shown in Figure 1 are found to be the energetically most favorable isomers among the numerous Au_6Y structures possessing a doublet ground state. All structures have a Y atom in the center and although they are now nonplanar, a direct correspondence of **6.1** and **6.2** with **5.1** and **5.2**, respectively, can be established. Compound **6.1** has C_{2v} symmetry and a $^2A_1$ state, which results from a Jahn–Teller distortion from higher D_{6h} symmetry. The planar C_{2v} form is characterized as a first-order saddle point, but is only marginally (0.02 eV) above **6.1**. An out-of-plane motion of the Y atom induces Au–Au bond breathing. The interconversion between different forms of **6.1**, which differ from each other by permutation of atomic positions, is also calculated to be a facile process having an energy barrier of only about 0.005 eV.[58] These findings indicate a nearly spontaneous and barrier-free pseudorotation rearrangement process. While the SOMO of **6.1** is delocalized over the entire Au skeleton, its LUMO is merely centered on the Y atom.

Compound **6.2** can be considered as arising from **6.1** by a strong out-of-plane distortion of one Au center, and it is calculated to be higher in energy than **6.1** by 0.35 eV using BP86, and 0.24 eV with CCSD(T) calculations. This calculated value is large enough to indicate a structural preference. Compounds **6.3** and **6.4** are almost degenerate in energy with **6.2**. The (slight) nonplanarity and low spin state of Au_6Y makes it markedly different from other Au_6M clusters with different dopants such as M = Ti, V, and Cr.[30]

The corresponding quartet counterpart of **6.1** has a C_{6v} shape (**6.6**) and a $^4A_1$ electronic state, and it is characterized by a relatively large doublet–quartet energy separation of −1.79 eV. The third isomer **6.3** has a lower-symmetry ground state (C_s, $^2A''$), the corresponding quartet structure (**6.5**) is slightly deformed (C_s, $^4A''$), and the doublet–quartet gap is reduced to −1.31 eV.

A peculiar feature of the observed FIR-MPD spectrum of Au_6YXe, displayed in Figure 7, is the broadening of the absorption bands, which is different from the observed spectra of all other Au_nYXe clusters discussed here. Upon comparing the calculated vibrational spectra of the four low-lying Au_6YXe isomers with experiment, we find that the spectrum of **6.1-Xe** agrees best. The origin of the band broadening can be accounted for by the low barriers, as discussed above, to inversion and permutation between different bond-stretching isomers of the most stable isomer **6.1-Xe**. The highly anharmonic potential and also the fluxional behavior most likely result in the broadened IR band.[58]

Figure 7. Comparison of the calculated (BP86/cc-pVDZ-PP) vibrational spectra of the four low-lying Au_6YXe isomers (relative energies in eV are given in parentheses) with the experimental FIR-MPD spectrum.

Au_7Y

The Au_7Y cluster is an example where the complex with two Xe atoms attached to the cluster is more abundant in the experiment than the one with only a single Xe atom. After exposure of the clusters to the FELIX laser beam, IR absorption can lead to the release of a single Xe atom from Au_7YXe_2, which results in a depletion of this complex in the molecular beam (see Figure 8). Figure 8 presents a zoom of the mass spectrum around Au_7Y and compares the intensity of the molecular beam before and after irradiation with FELIX at a specific frequency, 163 cm^{-1} in this case. This frequency corresponds to a vibrational resonance in Au_7YXe_2 resulting in the release of a single Xe atom and the depletion of the Au_7YXe_2 signal. However, for the complex with a single Xe atom we observe no depletion but only intensity growth at this frequency. This is found throughout the full spectral range: the intensity growth of Au_7YXe mirrors exactly the depletion of Au_7YXe_2, but no depletion signal for Au_7YXe is observed. For this reason it is only possible to deduce the structure from the experimental data of Au_7YXe_2.

Figure 1 shows the two structures labeled as **7.1** and **7.2** that are found to be the most stable Au_7Y isomers, again having a similar relative energy. The singlet ground state of **7.1** has a C_{2v} shape ($^1A_1$). In the triplet manifold, the Y atom undergoes an out-of-plane distortion, which results in the C_s form **7.4** ($^3A''$). The singlet–triplet energy gap of **7.1** is predicted to be −1.30 eV. The second isomer **7.2** ($^1A'$) is a C_s ring distorted from D_{7h} in keeping the Y atom centered at the middle. Nevertheless, the corresponding $D_{7h}-C_s$ energy difference is extremely small (∼0.03 eV). The triplet state of **7.2** strongly relaxes to a rather different form **7.3**, which has a triangle at the top connected with a chain of four Au atoms and a Y atom in
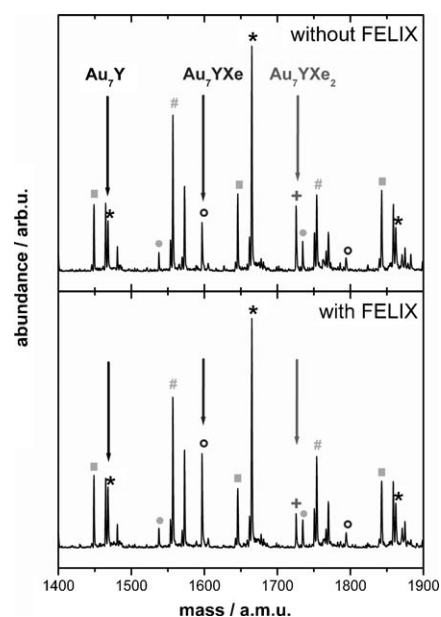
Figure 8. Mass spectra of Au_nY clusters produced with the source at 130 K and a fraction of enriched xenon in the helium carrier gas. The black asterisks indicate Au_nY ($n = 7$–9), the dark gray circles Au_nYXe ($n = 7$, 8), and the gray cross Au_7YXe_2. The other light gray symbols indicate extra yttrium doping, the hashes Au_nY_2, the squares Au_nY_3, and the triangles Au_nY_4. Extra peaks observed are oxygen contaminations. In the upper trace, the mass spectrum is shown without illumination by the FELIX beam, while in the lower trace the dissociation upon FELIX irradiation of one xenon atom from Au_7YXe_2 is observed.

the middle (C_s, $^3A''$). The singlet–triplet energy separation of **7.2** amounts to −1.02 eV.

Figure 9 shows IR spectra for Au_7YXe_2. For the most stable isomers **7.1** and **7.2**, the energy for binding the first Xe atom to Y is about ∼0.15 eV, which is much larger than when Xe
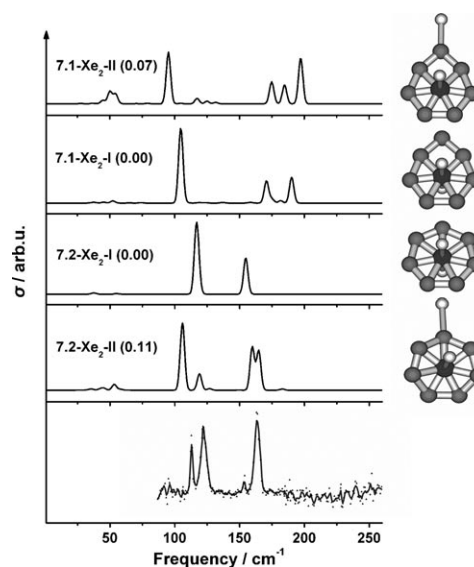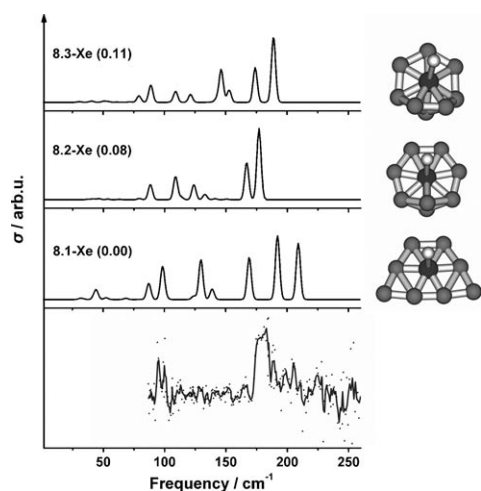

Figure 9. Comparison of the calculated (BP86/cc-pVDZ-PP) vibrational spectra of the low-lying Au_7YXe_2 isomers (relative energies in eV are given in parentheses) with the experimental FIR-MPD spectrum.

binds to Au (~0.05 eV). Similar to the other Au$_n$Y clusters, the attachment of Xe to Y is by far energetically preferred for both isomers. Our calculations also show that the second messenger atom tends to bind to Y as well (at an opposite position), and the resulting two-Xe complexes, namely **7.1-Xe$_2$-I** and **7.2-Xe$_2$-I**, are found to be the most stable Au$_7$YXe$_2$ complexes, which are again degenerate in energy. By comparing the available calculated vibrational spectra of the four low-lying isomers as seen in Figure 9, it can be concluded that both isomers **7.2-Xe$_2$-II** and **7.2-Xe$_2$-I** can be considered as main carriers of the vibrational motions. The bands calculated for **7.2-Xe$_2$-II** at around 160 and 165 cm^{-1} are mainly caused by Au−Y vibrational modes, which are degenerate and appear as a single peak in the spectrum of **7.2-Xe$_2$-I**. The intense bands centered at 106 (**7.2-Xe$_2$-II**) and 116 cm^{-1} (**7.2-Xe$_2$-I**) both correspond to the out-of-plane vibration of the Y atom (see Movies S3 and S4 in the Supporting Information).

From the combination of the calculated and experimentally obtained IR spectra we can conclude that the geometrical structure of Au$_7$Y appears in the experiment as a C_s ring slightly distorted from a D_{7h} structure in keeping the Y atom centered at the middle. As mentioned before, the corresponding D_{7h}−C_s energy difference is extremely small (~0.03 eV) and can be overcome by symmetrically adding two Xe atoms; therefore, we cannot exclude that **7.2-Xe$_2$-I** contributes to the IR spectrum.

Au$_8$Y

As shown in Figures 10 and 11, the experimental spectrum of the Au$_8$YXe complex has a poor signal-to-noise ratio and, except for the most intense band(s) situated around 180 (Au$_8$YXe) and 100 cm^{-1} (Au$_8$YXe$_2$), hardly any other resonance can be assigned. Upon comparing the relative abundance of the Au$_8$YXe complex with those of the clusters of other sizes, we notice a clearly lowered amount of this complex in the

Figure 10. Comparison of the calculated (BP86/cc-pVDZ-PP) vibrational spectra of the three lowest-lying Au$_8$YXe isomers (relative energies in eV are given in parentheses) with the experimental FIR-MPD spectrum.
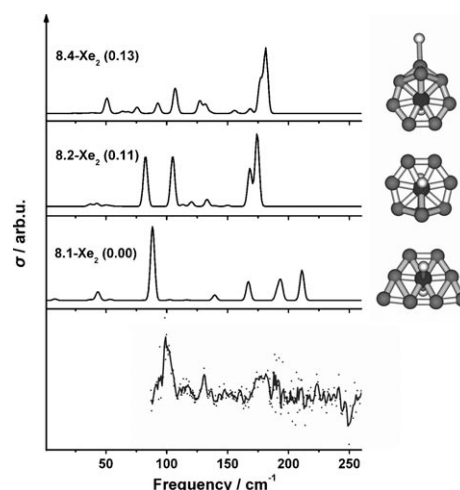
Figure 11. Comparison of the calculated (BP86/cc-pVDZ-PP) vibrational spectra of the three lowest-lying Au$_8$YXe$_2$ isomers (relative energies in eV are given in parentheses) with the experimental FIR-MPD spectrum.

mass distribution. After ionization, this cluster–rare-gas complex amounts to only 6% of the Au$_8$Y, whereas in Au$_9$Y this percentage amounts to almost 70%. The low intensity of Au$_8$YXe results in a very small signal in the mass spectrum and, correspondingly, in a very high noise level of the FIR-MPD spectrum. For this reason, attention must be paid when assigning a certain structure to Au$_8$Y. Again experimental IR spectra were observed for both one- and two-Xe complexes.

According to our DFT calculations, several isomers have similar relative energy (Figure S3 in the Supporting Information and Figure 1). The isomers **8.1**–**8.4** are predicted to be the most stable doublet-state structures of Au$_8$Y (Figure 1). While **8.1**, **8.3**, and **8.4** have C_s symmetry (^{2}A′), **8.2** has a C_{2v} form (^{2}B$_1$). Their SOMOs contain only very small contributions from Y (see Figure S1 in the Supporting Information). After one Xe atom binds to the Y atom of Au$_8$Y, the energy differences between the four isomers are enlarged. Let us take **8.1** and **8.4** as an example: the energy difference between them is increased from 0.08 to 0.19 eV upon Xe attachment. By comparing the computed spectra to the experimental results (Figure 10), it can be concluded that the **8.2-Xe** is seemingly the dominant isomer of Au$_8$YXe present in the molecular beam, and the intensive experimental band(s) around 180 cm^{-1} originate from Au−Y stretching vibrations.

It should be noted that Au$_8$Y can also bind two Xe atoms under the present instrumental conditions, and the comparison of the experimental and calculated vibrational spectra is shown in Figure 11. However, the signal of Au$_8$YXe$_2$ is even lower than that of Au$_8$YXe, and therefore prudence is called for while examining the experimental IR spectrum. The most intense band centered at 88 cm^{-1} of **8.1-Xe$_2$** agrees relatively well with the most pronounced band in the experiment; however, the bands around 180 cm^{-1} may be rather related to **8.2-Xe$_2$**. Thus, unfortunately no clear assignment can be made for the structure of Au$_8$Y.

Au$_9$Y

This cluster size also prefers a low-spin ground state, and the structures of three associated isomers on the singlet-state energy surface are shown in Figure 1, as well as two other isomers having the triplet state. Among a variety of local minima found for Au$_9$Y, **9.1** (C_{2v}, $^1A_1$) is predicted to be the most stable isomer, being energetically favored by 0.15 eV over **9.2** (D_{3h}, $^1A_1'$) and **9.3** (C_s, $^1A'$). The related singlet–triplet energy gap of **9.1** is predicted to be −1.00 eV. Contrary to what is found for Au$_8$Y, attachment of Xe to Y induces a decrease of the energy difference between low-lying isomers of Au$_9$Y. The binding energies of Xe to the Y of **9.2** and **9.3** are predicted as 0.16 and 0.13 eV, respectively, which are much larger than that of **9.1** (0.04 eV). It is surprising that the binding energy of Xe to the Y of **9.1** is so small, as it is different from those of other isomers discussed above. The Au-attached **9.1-Xe** turns out to be only ∼0.01 eV higher in energy than the Y-attached **9.1-Xe** complex (**9.1-Xe-I**).

A comparison of the IR spectra is shown in Figure 12, in which only one of the Au-attached **9.1-Xe** complexes, namely **9.1-Xe-II**, is plotted. The reason is that all these complexes
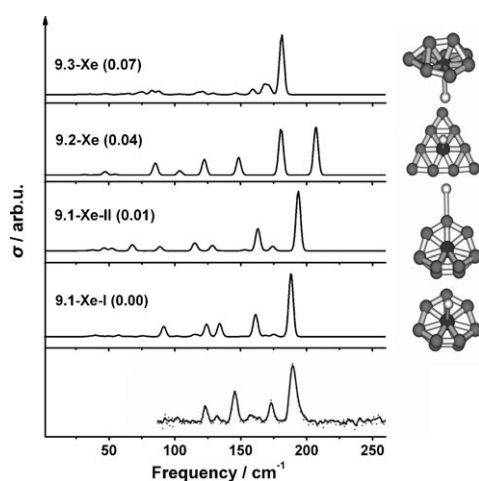
Figure 12. Comparison of the calculated (BP86/cc-pVDZ-PP) vibrational spectra of the four lowest-lying Au$_9$YXe isomers (relative energies in eV are given in parentheses) with the experimental FIR-MPD spectrum.

have similar relative energies and vibrational spectra. The experimental absorption bands of Au$_9$YXe are quite intense and narrow, which differs substantially from those of the neighboring cluster size Au$_8$YXe, and in addition, there is no Au$_9$YXe$_2$ complex detected in the experiment. The correspondence between the calculated spectrum of **9.1-Xe-I** and the experimental FIR-MPD spectrum is less convincing than for the other sizes. However, good matching for all but one mode (at 145 cm^{-1}) suggests that the main spectral carrier is identified, although the Au-attached Au$_9$YXe complexes most likely make a small contribution.

The Growth Pattern of Au$_n$Y Clusters

The number of structural isomers dramatically increases with increasing cluster size. Even though the search was carried out with a lot of care, it does not guarantee that for all clusters the global minimum has been located. However, in the present case of doped Au$_n$Y ($n=4$–9) clusters, the agreement between calculated IR spectra and experimental results lends support to the structural determination discussed above. Figure 1 gives a summary of the lowest-lying isomers of Au$_n$Y ($n=1$–9) identified by BP86/cc-pVDZ-PP calculations, and different lowest-lying isomers have been predicted for Au$_{6-9}$Y compared to what was reported previously in the literature.[56]

Au$_2$Y has a triangular form (AuYAu, C_{2v}), which is formed by adding a second Au atom to Y of the diatomic AuY. Addition of the third Au atom to the Y of Au$_2$Y leads to a D_{3h} symmetric Au$_3$Y. However, attachment of the fourth Au atom tends to break the high symmetry of Au$_3$Y and forms lower-symmetry structures **4.1** (C_s) and **4.2** (C_{2v}) containing similar energy, rather than a T_d form. Incorporation of the fifth Au atom to the Y of **4.1** leads to two low-lying Au$_5$Y forms, again with the same energy but different geometries, in which **5.1** is planar (C_{2v}) whereas **5.2** still keeps the C_s structure of **4.1**. Introduction of the sixth Au atom to **5.1** and **5.2**, at the Y center, produces **6.1** (C_{2v}) and **6.2** (C_s), respectively. Attachment of the seventh Au atom to the energetically preferred isomer **6.1** gives rise to two different species **7.1** and **7.2**, in which **7.1** is planar (C_{2v}) and **7.2** is nonplanar (C_s). Addition of the eighth Au atom to **7.1** and **7.2** yields several structures for Au$_8$Y with similar energies (see Figure 1, and also Figure S3 in the Supporting Information for more isomeric forms), in which the two most stable isomers **8.1** (C_s) and **8.2** (C_{2v}) bear, as in the previous cases, rather low symmetry. Au$_9$Y does not present many isomers with close energies as in Au$_8$Y, and the lowest-energy isomer **9.1** (C_{2v}) can be considered to be constructed by introducing the ninth Au atom into **8.2**.

A consistent feature that emerges from the set of assigned Au$_n$Y structures is that the Y atom prefers high coordination. Such behavior is different from that of most other transition-metal-doped gold clusters mentioned in the Introduction. Except for AuY and Au$_2$Y, the Y-doped gold clusters Au$_n$Y ($n=3$–9) adopt very different structural patterns from those of Au$_{n+1}$. In other words, doping one yttrium atom into pure gold clusters induces a full reconstruction of the structure for Au$_n$Y ($n=3$–9). Furthermore, we find that a small Au$_n$Y cluster can already adopt 3D shapes (see Figure 1), with the smallest 3D isomer being Au$_4$Y, whereas the pure Au$_n$ clusters prefer a planar form up to $n=11$.[7,8]

While the cluster grows, it is found that the larger the cluster size, the longer the average Au−Y bond length (see Table S1 in the Supporting Information). Attachment of Xe to Y also makes the Au−Y distance elongate further, and as a consequence a red shift of the corresponding IR band is induced.

The energy gap between frontier orbitals is usually considered as an important parameter to evaluate the electronic stability of small clusters. The size dependence of the HOMO/SOMO–LUMO gaps of pure Au$_n$ and doped Au$_n$Y clusters is
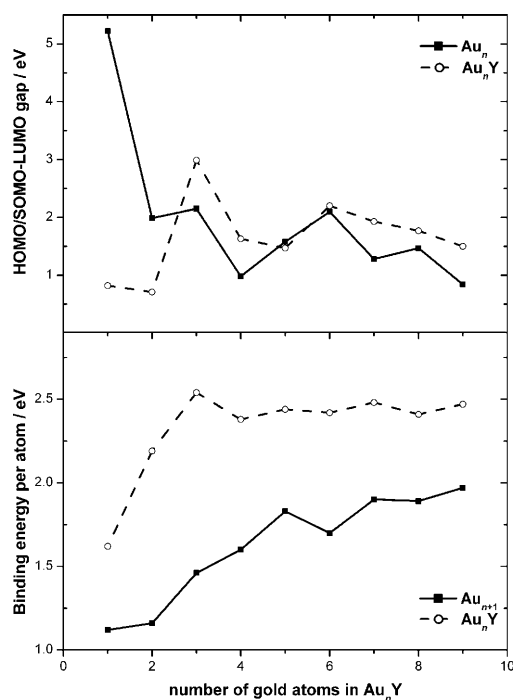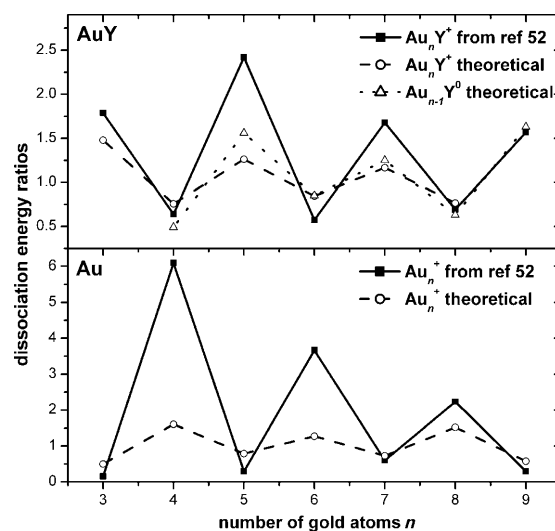
Figure 13. The HOMO/SOMO–LUMO gap and the average binding energy of the lowest-energy isomer for both Au_n and Au_nY ($n = 1$–9) calculated at the BP86/cc-pVDZ-PP level.
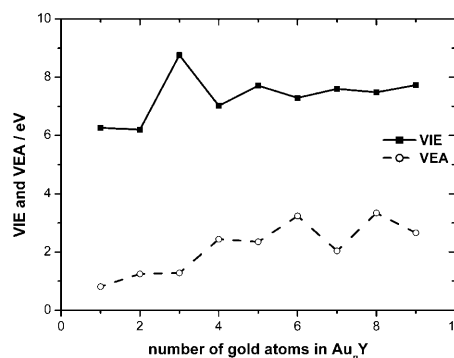

Figure 14. Comparison between the dissociation energy ratios obtained by delayed fragmentation[52] and theory for Au_nY^+ (upper trace) and Au_n^+ (lower trace). The dissociation energy ratios of Au_nY are also included to allow comparison of these values with those of their cationic counterparts with the same number of valence electrons.

Figure 15. Vertical ionization energy (VIE) and vertical electron affinity (VEA) as a function of the number of gold atoms for Au_nY ($n = 1$–9). All the data were obtained with BP86/cc-pVDZ-PP.

shown in Figure 13. Noticeable peaks are found at $n = 3$ and 6 for both series, which suggests that Au_3, Au_6, Au_3Y, and Au_6Y have relatively higher chemical stability than the neighboring clusters. Except for $n = 1$, 2, and 5, the HOMO/SOMO–LUMO gap is found to be enlarged upon incorporation of a Y atom into Au_n, thus indicating that the doped clusters are more stable than their bare counterparts.

The clusters' stability can also be discussed on the basis of the binding energy per atom. Figure 13 points out that the average binding energy of Au_nY shows odd–even oscillations from $n = 2$, with higher abundance for the odd sizes at $n = 3$, 5, 7, and 9. The average binding energy of Au_nY is higher than that of Au_{n+1}, thus implying stronger interaction between the atoms in Au_nY, which can be attributed to the enhancement of the binding between Y and Au due to ionic bonding. In fact, the NBO charge analysis shows that the Y atom is always positively charged in Au_nY (Table S3 in the Supporting Information), which suggests that there is an effective charge transfer from Y to Au.

Additionally we compared the calculated dissociation energy rations D'_{n+1}/D'_n with the experimental ones obtained from previous investigations.[52] The structures of the lowest isomers of Au_n^+ ($n = 3$–10) were taken from the literature[9] and reoptimized with BP86/cc-pVDZ-PP, while the Au_nY^+ ($n = 2$–9) were obtained by optimizing the cationic isomer starting from the four lowest Au_nY isomers (Figure S4 in the Supporting Information). It should be noted that these doped counterparts may not yet be the global minima. From Figure 14 it is clear that the experimentally observed odd–even alternations are confirmed by theory. We show a comparison between the calculat-

ed dissociation energies of Au_n^+ and Au_nY^+ with the experimental energies from ref. [52], and include the calculated dissociation energies of Au_nY from the structures predicted in this article.

The vertical ionization energy (VIE) and vertical electron affinity (VEA) of Au_nY were also calculated, and both patterns show odd–even oscillations (Figure 15). For the VIE, higher values are found for $n = 1$, 3, 5, 7, and 9, with the opposite odd–even effect for the VEA sequence and higher stability for the anions Au_2Y^-, Au_4Y^-, Au_6Y^-, and Au_8Y^-.

Conclusions

In this combined study, we employed FIR-MPD spectroscopy and quantum chemical calculations (BP86 and CCSD(T) methods) to probe the spectroscopic, geometric, and electronic properties of yttrium-doped gold clusters Au_nY ($n = 1$–9). For each isomeric system considered, a large number of possible

structures were explored. Comparison of the observed and calculated vibrational spectra allowed the basic structural features of the most likely isomers to be determined. The isomers whose vibrational spectra agree best with experiment are consistently the energetically most stable forms, except for Au$_7$Y and Au$_8$Y where the computational energy differences between low-energy structures are very small. Attachment of xenon to the Au$_n$Y cluster can induce a band shift, occasionally also a splitting of the band, and can have a notable influence on the band intensities in the IR spectra and in some cases ($n = 4$, 8) on the symmetry of the cluster.

In contrast to pure gold clusters, small Au$_n$Y cluster sizes, in particular Au$_4$Y, show a 3D shape. Several other sizes of Au$_n$Y ($n = 5$–8) adopt a 2D shape in their lower-lying isomers, although there is a fairly small distortion from perfectly planar structures. However, for $n = 5$ and 8, low-lying 3D structures also emerge with an energy content similar to their 2D counterparts. The largest Y-doped species studied here, Au$_9$Y, prefers a 3D shape. The Y atom invariably prefers high coordination, which is different from the behavior of other transition-metal-doped gold clusters. Overall, the presence of a dopant is predicted to enhance considerably the thermodynamic stability of the gold clusters for many cluster sizes.

Acknowledgements

Keywords: cluster compounds · density functional calculations · gold · IR spectroscopy · yttrium

[1] M. Valden, X, Lai, D. W. Goodman, *Science* **1998**, *281*, 1647.
[2] S. Chrétien, S. K. Buratto, H. Metiu, *Curr. Opin. Solid State Mater. Sci.* **2007**, *11*, 62.
[3] F. R. F. Fan, A. J. Bard, *Science* **1997**, *277*, 1791.
[4] C. Zhang, B. Yoon, U. Landman, *J. Am. Chem. Soc.* **2007**, *129*, 2228.
[5] B. Yoon, H. Häkkinen, U. Landman, A. S. Wörz, J.-M. Antonietti, S. Abbet, K. Judai, U. Heiz, *Science* **2005**, *307*, 403.
[6] A. A. Herzing, C. J. Kiely, A. F. Carley, P. Landon, G. J. Hutchings, *Science* **2008**, *321*, 1331.
[7] X. B. Li, H. Y. Wang, X. D. Yang, Z. H. Zhu, Y. J. Tang, *J. Chem. Phys.* **2007**, *126*, 084 505.
[8] E. M. Fernández, J. M. Soler, I. L. Garzón, L. C. Balbás, *Phys. Rev. B* **2004**, *70*, 165 403.
[9] S. Gilb, P. Weis, F. Furche, R. Ahlrichs, M. M. Kappes, *J. Chem. Phys.* **2002**, *116*, 4094.
[10] H. Woldeghebriel, A. Kshirsagar, *J. Chem. Phys.* **2007**, *127*, 224 708.
[11] F. Furche, R. Ahlrichs, P. Weis, C. Jacob, S. Gilb, T. Bierweiler, M. M. Kappes, *J. Chem. Phys.* **2002**, *117*, 6982.
[12] M. P. Johansson, A. Lechtken, D. Schooss, M. M. Kappes, F. Furche, *Phys. Rev. A* **2008**, *77*, 053 202.
[13] P. Pyykkö, *Angew. Chem.* **2004**, *116*, 4512; *Angew. Chem. Int. Ed.* **2004**, *43*, 4412.
[14] P. Pyykkö, *Chem. Rev.* **1988**, *88*, 563.
[15] P. A. Christiansen, W. C. Ermler, K. S. Pitzer, *Annu. Rev. Phys. Chem.* **1985**, *36*, 407.
[16] C. Majumder, S. K. Kulshreshtha, *Phys. Rev. B* **2006**, *73*, 155 427.
[17] C. Majumder, *Phys. Rev. B* **2007**, *75*, 235 409.
[18] B. Kiran, X. Li, H.-J. Zhai, L.-F. Cui, L.-S. Wang, *Angew. Chem.* **2004**, *116*, 2177; *Angew. Chem. Int. Ed.* **2004**, *43*, 2125.
[19] M. Walter, H. Häkkinen, *Phys. Chem. Chem. Phys.* **2006**, *8*, 5407.
[20] Q. Sun, Q. Wang, G. Chen, P. Jena, *J. Chem. Phys.* **2007**, *127*, 214 706.
[21] C. Majumder, A. K. Kandalam, P. Jena, *Phys. Rev. B* **2006**, *74*, 205 437.
[22] L. M. Wang, S. Bulusu, W. Huang, R. Pal, L. S. Wang, X. C. Zeng, *J. Am. Chem. Soc.* **2007**, *129*, 15 136.
[23] R. Pal, L. M. Wang, W. Huang, L. S. Wang, X. C. Zeng, *J. Am. Chem. Soc.* **2009**, *131*, 3396.
[24] W. Fa, J. M. Dong, *J. Chem. Phys.* **2008**, *128*, 144 307.
[25] L. F. Cui, Y. C. Lin, D. Sundholm, L. S. Wang, *J. Phys. Chem. A* **2007**, *111*, 7555.
[26] H. Tanaka, S. Neukermans, E. Janssens, R. E. Silverans, P. Lievens, *J. Chem. Phys.* **2003**, *119*, 7115.
[27] H. Tanaka, S. Neukermans, E. Janssens, R. E. Silverans, P. Lievens, *J. Am. Chem. Soc.* **2003**, *125*, 2862.
[28] D. W. Yuan, Y. Wang, Z. Zeng, *J. Chem. Phys.* **2005**, *122*, 114 310.
[29] W. Q. Tian, M. F. Ge, F. L. Gu, T. Yamada, Y. Aoki, *J. Phys. Chem. A* **2006**, *110*, 6285.
[30] X. Li, B. Kiran, L. F. Cui, L. S. Wang, *Phys. Rev. Lett.* **2005**, *95*, 253 401.
[31] M. X. Chen, X. H. Yan, *J. Chem. Phys.* **2008**, *128*, 174 305.
[32] L. Gagliardi, *J. Am. Chem. Soc.* **2003**, *125*, 7504.
[33] T. K. Ghanty, K. R. S. Chandrakumar, S. K. Ghosh, *J. Chem. Phys.* **2004**, *120*, 11 363.
[34] P. Pyykkö, N. Runeberg, *Angew. Chem.* **2002**, *114*, 2278; *Angew. Chem. Int. Ed.* **2002**, *41*, 2174.
[35] S. Zorriasatein, K. Joshi, D. G. Kanhere, *J. Chem. Phys.* **2008**, *128*, 184 314.
[36] Y. Gao, S. Bulusu, X. C. Zeng, *ChemPhysChem* **2006**, *7*, 2275.
[37] Y. Gao, S. Bulusu, X. C. Zeng, *J. Am. Chem. Soc.* **2005**, *127*, 15 680.
[38] J. Long, Y. X. Qiu, X. Y. Chen, S. G. Wang, *J. Phys. Chem. C* **2008**, *112*, 12 646.
[39] X. Li, B. Kiran, J. Li, H. J. Zhai, L. S. Wang, *Angew. Chem.* **2002**, *114*, 4980; *Angew. Chem. Int. Ed.* **2002**, *41*, 4786.
[40] H. J. Zhai, J. Li, L. S. Wang, *J. Chem. Phys.* **2004**, *121*, 8369.
[41] L. M. Wang, S. Bulusu, H. J. Zhai, X. C. Zeng, L. S. Wang, *Angew. Chem.* **2007**, *119*, 2973; *Angew. Chem. Int. Ed.* **2007**, *46*, 2915.
[42] L. M. Wang, J. Bai, A. Lechtken, W. Huang, D. Schooss, M. M. Kappes, X. C. Zeng, L. S. Wang, *Phys. Rev. B* **2009**, *79*, 033 413.
[43] L. M. Wang, R. Pal, W. Huang, X. C. Zeng, L. S. Wang, *J. Chem. Phys.* **2009**, *130*, 051 101.
[44] R. Ferrando, A. Fortunelli, R. L. Johnston, *Phys. Chem. Chem. Phys.* **2008**, *10*, 640.
[45] W. A. de Heer, *Rev. Mod. Phys.* **1993**, *65*, 611.
[46] I. Katakuse, T. Ichihara, Y. Fujita, T. Matsuo, T. Sakurai, H. Matsuda, *Int. J. Mass Spectrom. Ion Processes* **1985**, *67*, 229.
[47] E. Janssens, S. Neukermans, P. Lievens, *Curr. Opin. Solid State Mater. Sci.* **2004**, *8*, 185.
[48] S. Neukermans, E. Janssens, H. Tanaka, R. E. Silverans, P. Lievens, *Phys. Rev. Lett.* **2003**, *90*, 033 401.
[49] E. Janssens, H. Tanaka, S. Neukermans, R. E. Silverans, P. Lievens, *Phys. Rev. B* **2004**, *69*, 085 402.
[50] E. Janssens, H. Tanaka, S. Neukermans, R. E. Silverans, P. Lievens, *New J. Phys.* **2003**, *5*, 46.
[51] W. Bouwen, F. Vanhoutte, F. Despa, S. Bouckaert, S. Neukermans, L. T. Kuhn, H. Weidele, P. Lievens, R. E. Silverans, *Chem. Phys. Lett.* **1999**, *314*, 227.
[52] N. Veldeman, E. Janssens, K. Hansen, J. De Haeck, R. E. Silverans, P. Lievens, *Faraday Discuss.* **2008**, *138*, 147.

[53] P. Gruene, A. Fielicke, G. Meijer, E. Janssens, V. T. Ngan, M. T. Nguyen, P. Lievens, *ChemPhysChem* **2008**, *9*, 703.

[54] J. T. Lyon, P. Gruene, A. Fielicke, G. Meijer, E. Janssens, P. Claes, P. Lievens, *J. Am. Chem. Soc.* **2009**, *131*, 1115.

[55] P. Gruene, D. M. Rayner, B. Redlich, A. F. G. van der Meer, J. T. Lyon, G. Meijer, A. Fielicke, *Science* **2008**, *321*, 674.

[56] H. P. Mao, H. Y. Wang, Z. H. Zhu, Y. J. Tang, *Acta Phys. Sin.* **2006**, *55*, 4542.

[57] J. J. Guo, J. X. Yang, D. Dong, *Phys. B* **2008**, *403*, 4033.

[58] L. Lin, T. Höltzl, P. Gruene, P. Claes, G. Meijer, A. Fielicke, P. Lievens, M. T. Nguyen, *ChemPhysChem* **2008**, *9*, 2471.

[59] G. von Helden, D. van Heijnsbergen, G. Meijer, *J. Phys. Chem. A* **2003**, *107*, 1671.

[60] A. Fielicke, G. Meijer, G. von Helden, *J. Am. Chem. Soc.* **2003**, *125*, 3659.

[61] E. Janssens, P. Gruene, G. Meijer, L. Wöste, P. Lievens, A. Fielicke, *Phys. Rev. Lett.* **2007**, *99*, 063401.

[62] D. Oepts, A. F. G. van der Meer, P. W. van Amersfoort, *Infrared Phys. Technol.* **1995**, *36*, 297.

[63] W. Bouwen, P. Thoen, F. Vanhoutte, S. Bouckaert, F. Despa, H. Weidele, R. E. Silverans, P. Lievens, *Rev. Sci. Instrum.* **2000**, *71*, 54.

[64] M. Okumura, L. I. Yeh, Y. T. Lee, *J. Chem. Phys.* **1985**, *83*, 3705.

[65] K. R. Asmis, J. Sauer, *Mass Spectrom. Rev.* **2007**, *26*, 542.

[66] A. Fielicke, G. von Helden, G. Meijer, *Eur. Phys. J. D* **2005**, *34*, 83.

[67] R. G. Parr, W. T. Yang, *Density Functional Theory of Atoms and Molecules*, Oxford University Press, Oxford, **1989**.

[68] A. D. Becke, *Phys. Rev. A* **1988**, *38*, 3098.

[69] J. P. Perdew, *Phys. Rev. B* **1986**, *33*, 8822.

[70] K. A. Peterson, C. Puzzarini, *Theor. Chem. Acc.* **2005**, *114*, 283.

[71] K. A. Peterson, D. Figgen, M. Dolg, H. Stoll, *J. Chem. Phys.* **2007**, *126*, 124101.

[72] K. A. Peterson, D. Figgen, E. Goll, H. Stoll, M. Dolg, *J. Chem. Phys.* **2003**, *119*, 11113.

[73] J. A. Pople, M. Head-Gordon, K. Raghavachari, *J. Chem. Phys.* **1987**, *87*, 5968.

[74] *Gaussian 03, Revision C.02*, M. J. Frisch, G. W. Trucks, H. B. Schlegel, G. E. Scuseria, M. A. Robb, J. R. Cheeseman, J. A. Montgomery, Jr., T. Vreven, K. N. Kudin, J. C. Burant, J. M. Millam, S. S. Iyengar, J. Tomasi, V. Barone, B. Mennucci, M. Cossi, G. Scalmani, N. Rega, G. A. Petersson, H. Nakatsuji, M. Hada, M. Ehara, K. Toyota, R. Fukuda, J. Hasegawa, M. Ishida, T. Nakajima, Y. Honda, O. Kitao, H. Nakai, M. Klene, X. Li, J. E. Knox, H. P. Hratchian, J. B. Cross, V. Bakken, C. Adamo, J. Jaramillo, R. Gomperts, R. E. Stratmann, O. Yazyev, A. J. Austin, R. Cammi, C. Pomelli, J. W. Ochterski, P. Y. Ayala, K. Morokuma, G. A. Voth, P. Salvador, J. J. Dannenberg, V. G. Zakrzewski, S. Dapprich, A. D. Daniels, M. C. Strain, O. Farkas, D. K. Malick, A. D. Rabuck, K. Raghavachari, J. B. Foresman, J. V. Ortiz, Q. Cui, A. G. Baboul, S. Clifford, J. Cioslowski, B. B. Stefanov, G. Liu, A. Liashenko, P. Piskorz, I. Komaromi, R. L. Martin, D. J. Fox, T. Keith, M. A. Al-Laham, C. Y. Peng, A. Nanayakkara, M. Challacombe, P. M. W. Gill, B. Johnson, W. Chen, M. W. Wong, C. Gonzalez, J. A. Pople, Gaussian, Inc., Wallingford, CT, **2004**.

[75] MOLPRO is a package of ab initio programs designed by H. J. Werner, P. J. Knowles: R. D. Amos, A. Bernhardsson, A. Berning, P. Celani, D. L. Cooper, M. J. O. Deegan, A. J. Dobbyn, F. Eckert, C. Hampel, G. Hetzer, P. J. Knowles, T. Korona, R. Lindh, A. W. Lloyd, S. J. McNicholas, F. R. Manby, W. Meyer, M. E. Mura, A. Nicklass, P. Palmieri, R. Pitzer, G. Rauhut, M. Schutz, U. Schumann, H. Stoll, A. J. Stone, R. Tarroni, T. Thorsteinsson, H.-J. Werner, MOLPRO, version 2006.1, **2006**.

[76] E. D. Glendening, J. K. Badenhoop, A. E. Reed, J. E. Carpenter, J. A. Bohmann, C. M. Morales, F. Weinhold, NBO5.G, Theoretical Chemistry Institute, University of Wisconsin, Madison, WI, **2001**.

[77] J. P. Merrick, D. Moran, L. Radom, *J. Phys. Chem. A* **2007**, *111*, 11683.

[78] R. Gehrke, P. Gruene, A. Fielicke, G. Meijer, K. Reuter, *J. Chem. Phys.* **2009**, *130*, 034306.